Article

Oxidative Stress Alters the Morphology and Toxicity of Aortic Medial Amyloid

Hannah A. Davies,[1] Marie M. Phelan,[1,2] Mark C. Wilkinson,[1] Raymond Q. Migrino,[3] Seth Truran,[3] Daniel A. Franco,[3] Lu-Ning Liu,[1] Christopher J. Longmore,[1] and Jillian Madine[1,*]

[1]Institute of Integrative Biology and [2]Technology Directorate, University of Liverpool, Liverpool, UK; and [3]Office of Research, Phoenix Veterans Affairs Health Care System, Phoenix, Arizona

ABSTRACT The aggregation and fibril deposition of amyloid proteins have been implicated in a range of neurodegenerative and vascular diseases, and yet the underlying molecular mechanisms are poorly understood. Here, we use a combination of cell-based assays, biophysical analysis, and atomic force microscopy to investigate the potential involvement of oxidative stress in aortic medial amyloid (AMA) pathogenesis and deposition. We show that medin, the main constituent of AMA, can induce an environment rich in oxidative species, increasing superoxide and reducing bioavailable nitric oxide in human cells. We investigate the role that this oxidative environment may play in altering the aggregation process of medin and identify potential post-translational modification sites where site-specific modification and interaction can be unambiguously demonstrated. In an oxidizing environment, medin is nitrated at tyrosine and tryptophan residues, with resultant effects on morphology that lead to longer fibrils with increased toxicity. This provides further motivation to investigate the role of oxidative stress in AMA pathogenicity.

INTRODUCTION

Aortic medial amyloid (AMA) is found in 97% of Caucasian individuals over the age of 50 and is the most common form of localized amyloid. It is found in close association with the internal elastic lamina, an elastin-rich layer that supports the endothelium and allows for arterial stretch (1,2). The main constituent of AMA is a 50 amino acid polypeptide called medin (3). Experimental evidence suggests that prefibrillar intermediates of medin are toxic to aortic endothelial cells in vitro (4) and may underlie the pathogenesis of sporadic thoracic aortic aneurysm in vivo through weakening of the aortic wall (5). Molecular information about the mechanisms that trigger medin aggregation and the formation of insoluble fibrils is sparse. Posttranslational modifications occur in vivo in many proteins and may represent a mechanism for modulating fibril formation.

Oxidative or nitrative stress results when there is a loss of balance between oxidant formation and antioxidant removal through a defense mechanism (e.g., superoxide dismutase) (6). When this physiological balance is weakened, nitroxidative stress emerges and causes damage, including nitration of tyrosine residues. Superoxide is produced in endothelial cells, smooth muscle cells, and cardiomyocytes, and nitric oxide (NO) plays a role in maintaining cellular homeostasis in the cardiovascular system (7–9). Tyrosine nitration is a normal process, with low levels found in standard cells. However, elevated levels of 3-nitrotyrosine have been reported in a range of human pathologies and animal models of diseases, including atherosclerosis (10) and myocardial malfunction (11), and upon aging (12). Nitration has been shown to modulate the aggregation properties of proteins associated with neurodegenerative diseases, such as tau (13), β-amyloid (14), and α-synuclein (15,16), and has been identified in disease-associated amyloid deposits (17,18). Nitrotyrosine levels are significantly higher in human atherosclerotic lesions associated with coronary heart disease, and decrease after treatment with statin, an indirect antioxidant (19).

In this work, we assess a possible driving factor in amyloid formation, specifically, whether nitration of medin alters its in vitro aggregation and toxicological properties. As medin is found in an environment rich with oxidative species, we propose that nitration could play a role in mediating fibril formation of the protein, as has been shown for other amyloid proteins. We present data that suggest that medin could induce oxidative conditions in vivo and investigate the role that these conditions play in AMA pathogenicity.

MATERIALS AND METHODS

Expression of protein

Unlabeled and ^{13}C, ^{15}N isotope-labeled medin was expressed using pOPINS-medin in Lemo 21 (DE3) cells (20). Cells were induced at OD_{600} 0.8–1.0 with isopropyl-β-D-thiogalacto-pyranoside (1 mM) for 16 h at 20°C. Cells were harvested by centrifugation (3,000 × g, 20 min, 4°C). Pellets were resuspended in 6 M guanidine hydrochloride (GdmCl), 0.5 M

Submitted June 16, 2015, and accepted for publication October 13, 2015.

*Correspondence: j.madine@liv.ac.uk

Editor: David Eliezer.

0006-3495/15/12/2363/8

http://dx.doi.org/10.1016/j.bpj.2015.10.034

sodium phosphate, 20 mM NaCl, pH 8.0, and frozen at −20°C. The cells were homogenized and cell debris was removed by centrifugation (19,000 × *g*, 15 min, 4°C). The supernatant was loaded onto a 5 mL Ni^{2+}-NTA column and washed with 4 column volumes (CV) of 6 M GdmCl, pH 8, followed by 4 CV of 6 M GdmCl, pH 6. It was eluted with 3 CV of 6 M GdmCl, pH 2, and stored at −20°C. Fusion protein was buffer exchanged into 20 mM Tris-Cl, 0.5 M NaCl, pH 7.4, and the His6-SUMO tag was removed by incubation with SUMO protease I at 4°C for 3 h. The cleavage mixture was then passed through a 5 mL Ni^{2+}-NTA column and the flow-through containing medin was collected and characterized by matrix-assisted laser desorption and ionization mass spectrometry. Medin was buffer exchanged for different applications as described below.

NO and superoxide production

Human umbilical vein endothelial cells (HUVECs; Lonza, Walkersville, MD; passages 4–10) were exposed to medin (0.1–5 μM in 20 mM sodium phosphate, 20 mM NaCl, pH 7.4) for 20–24 h. NO gas was measured with the use of a Sievers NO analyzer (GE Analytical Instruments, Boulder, CO) and normalized to the cell count. In separate experiments, HUVECs were treated for 60 min with medin (5 μM ± pegylated superoxide dismutase (PEGSOD, 300 U/mL)), as well as untreated media control. After 45 min, acetylcholine (10^{-4} M) was added to the treatment media and incubated for the remaining 15 min. After treatment, the cells were washed with cold PBS, fixed with 4% paraformaldehyde in PBS and cold 100% methanol, and then washed again and stained in 5 μM dihydroethidium (Molecular Probes, Eugene, OR). Coverslips were attached to slides with SlowFade gold antifade reagent (Thermo Fisher Scientific, Waltham, MA) and imaged on an EVOS FL Auto imaging system (Life Technologies, Eugene, OR) using an RFP light cube (excitation 531/40, emission 593/40). Images were analyzed using ImageJ Java-based image processing and analysis software (NIH, Bethesda, MD).

Nitration of medin

Nitration was carried out as previously described using peroxynitrite (21,22). Medin was exchanged into nitration buffer (100 mM potassium phosphate, 25 mM sodium bicarbonate, pH 7.4, 0.1 mM diethylenetriaminepentaacetic acid). Peroxynitrite (Cayman Chemical, Ann Arbor, MI) was added to the required final molar ratio (0.5–50 excess for dot-blot, 10 excess for all other experiments) and vortexed. Nitration was monitored by measuring an increase in absorbance at 430 nm.

Mass spectrometry

Each sample was infused into the nano-electrospray source of the mass spectrometer (Q-Tof micro; Waters, Hertfordshire, UK) at a flow rate of 50 μL/h via a gas-tight syringe. The positive ion mass spectrum of the sample was scanned in the range of 80–2000 m/z using a scan time of 1 s and a data acquisition time of 5 min. MassLynx MaxEnt1 was then used to convert the summed multiply charged spectrum to a molecular mass spectrum.

Reverse-phase high-performance liquid chromatography

Control or nitrated medin was digested for 16 h at 25°C with mass-spectrometry-grade trypsin in the presence of 2 M urea. The resulting peptides were made up to 0.5% (v/v) in trifluoroacetic acid (TFA), centrifuged at 10,000 × *g* for 5 min, and applied to an Agilent Eclipse C18 reverse-phase high-performance liquid chromatography (RP-HPLC) column (100 × 2.1 mm) equilibrated in 0.08% TFA. Peptides were separated with a two-part acetonitrile gradient in 0.08% TFA (0–40% over 25 min, and then 40–65% over 15 min). Elution was monitored at 214 nm.

NMR

For nitration analysis, spectra were acquired using ^{13}C, ^{15}N medin at 25°C for 20 μM medin in nitration buffer, pH 6.8, containing 10% (v/v) $^{2}H_2O$ on a Bruker AVANCE III 600 MHz equipped with a 5 mm cryoprobe. ^{1}H-^{15}N heteronuclear single quantum coherence (HSQC) spectra were collected with 32 transients and a resolution of 20.3 Hz in the indirect dimension, allowing clearly resolved backbone peaks to be obtained. ^{1}H-^{13}C aromatic constant-time transverse-relaxation-optimized spectroscopy (CT-TROSY) spectra were collected for the aromatic HC resonances with 32 transients and a resolution of 45.27 Hz in the indirect dimension. Spectra were collected after 1 h of incubation in nitration buffer ± a 10-fold molar excess of peroxynitrite. The sample pH was checked before each measurement. Spectra were processed using Topspin 3.1 (Bruker) and assignment was carried out in CCPN Analysis (23) using chemical-shift values from Biological Magnetic Resonance Bank entry 26576 (24). The maximum change in chemical shift was calculated based on a combination of proton and nitrogen chemical-shift changes:

$$\Delta\delta = \left\{(\Delta H_N)^2 + (0.15\Delta N_H)^2\right\}^{1/2}. \quad (1)$$

Shifts considered noteworthy were identified as >1 SD for total shifts observed.

Medin aggregation

Medin (control and nitrated) was buffer exchanged using a PD10 column from nitration buffer into aggregation buffer (20 mM sodium phosphate, 20 mM NaCl, pH 7.4) and incubated at 20–50 μM at 37°C.

Thioflavin T (ThT) fluorescence assays were carried out on a Flexstation 3 microplate reader (Molecular Devices Ltd., Sunnyvale, CA) for 20 μM medin with 2 μM ThT. Experiments were carried out in 96-well, black-walled, clear-bottomed microplates. Data were recorded every 5 min using the bottom read mode, with excitation at 450 nm and emission at 485 nm.

Synchrotron radiation circular dichroism (SRCD) spectra were acquired for 50 μM medin in a 0.2 mm-pathlength quartz cuvette from 190 nm to 260 nm on beamline B23 of the Diamond Light Source (Oxford, UK) (25), in 1 nm increments using a 0.5 mm slit width. Spectra were recorded as the average of four scans and are presented after subtraction of buffer control spectra.

Atomic force microscopy

After incubation at 50 μM at 37°C for 2 days, samples were incubated in 20 μL absorption buffer (10 mM Tris-HCl pH 7.5, 150 mM KCl, 25 mM $MgCl_2$) (26) on freshly cleaved mica for 15 min and then rinsed with sterile-filtered deionized water before drying. Samples were imaged in PeakForce QNM mode in air on a Bruker Multimode 8 atomic force microscope equipped with a 160 μm scanner (J-scanner) using ScanAsyst-Air probes (k = 0.4 N/m). Images were recorded at 512 × 512 pixels and the atomic force microscopy (AFM) data were analyzed using the Bruker NanoScope analysis software.

Cell viability

Primary human aortic smooth muscle cells (HAoSMCs; Promocell, Heidelberg, Germany) were plated on 96-well plates at 4000 cells/well and grown for 24 h. Medin samples (control and nitrated, preincubated at 50 μM as described above) were diluted to 20 μM in buffer and added to the cells.

After incubation for 48 h, 10 μL of Cell Counting Kit-8 (CCK-8) solution was added and further incubated for 2 h. Absorbance was then measured at 450 nm. Percentage cell viability was calculated based on the absorbance measured relative to that of cells exposed to buffer alone.

RESULTS AND DISCUSSION

Addition of 5 μM medin to HUVECs caused a significant increase in superoxide (O_2^-) production ($p = 0.037$; Fig. 1 *A*), which was attenuated by addition of PEGSOD. Addition of medin to HUVECs caused a concentration-dependent decrease in NO production, with a significant reduction for 5 μM medin ($p = 0.009$; Fig. 1 *B*). NO can be converted to various other reactive nitrogen species (RNS) or reactive oxygen species (ROS) depending on the microenvironment; therefore, the reduction in NO production observed here is indicative of a reduction in bioavailable NO. In the presence of O_2^-, NO can be converted into peroxynitrite ($ONOO^-$) (27) a powerful nitrating reagent in vivo (7). Taken together, these data show that addition of 5 μM medin induced an increase in superoxide (Fig. 1 *A*) and reduced bioavailable NO (Fig. 1 *B*) in HUVECs, consistent with an increase in peroxynitrite production. These data indicate that medin could induce production of the components required for peroxynitrite production in vivo, in turn providing an ROS/RNS-rich environment that enhances the probability of tyrosine nitration.

The gold standard assay for superoxide production using dihydroethidium is HPLC (28,29), which was not used in this study. Although fluorescence microscopy cannot distinguish between signals from 2-hydroxyethidium (produced from interaction with superoxide anion) and ethidium (a dihydroethidium product not related to superoxide production), the reduction of signal in medin-treated cells cotreated with PEGSOD (a modified metalloprotein that specifically catalyzes the superoxide anion) suggests that the difference in fluorescent signal is due to 2-hydroxyethidium and not ethidium. This approach was previously used by other investigators to measure specifically superoxide production in cells/tissues (30,31).

Medin has a single tyrosine residue at position 16, and this residue was predicted to be nitrated (0.737, high-threshold cutoff 0.725) using the GPS-YNO2 prediction software (32). Further experiments provided experimental proof that this residue undergoes nitration. Exposure to peroxynitrite caused nitration to occur in a concentration-dependent manner (0.5–50 excess), as assessed by an increase in absorbance at 430 nm (33) and 3-nitrotyrosine antibody reactivity (Fig. S1 in the Supporting Material). Exposure to peroxynitrite can also cause nitration and oxidation of tryptophan residues (34,35). An examination of the peroxynitrite-treated medin sample (10 excess) by electrospray ionization mass spectrometry suggested the addition of $3NO_2$ groups (+135 Da; Fig. 2) consistent with nitration of all three susceptible residues (Y16, W11, and W21). There was an additional peak (+106 Da) that could represent a subsequent loss of two oxygen and further reduction (addition of two hydrogens, −~30 Da) due to photodecomposition under electrospray ionization conditions (Fig. 2 *C*, *inset*) (13,36). Alternatively, the peak at +106 could be derived from the addition of $2NO_2$ groups and a single tryptophan oxidation (37). Additional peaks were likely due to additional oxidation events in a small proportion of the sample. Trypsin digestion followed by RP-HPLC and mass spectrometry of control medin produced three predominant peptides, with mass-spectrometry-confirmed masses of 2841, 1145, and 968, corresponding to residues 5–30, 31–41, and 42–50 (Fig. 2 *B*, peaks 1–3, respectively). After nitration, peak 1 was broadened, whereas the other peaks remained unaltered (Fig. 2 *D*), confirming that all modifications had occurred within the peptide corresponding to residues 5–30, encompassing Y16, W11, and W21.

To gain residue-specific information and confirm nitration of tryptophan residues, we obtained ^1N-^{15}N HSQC spectra in nitration buffer before and after exposing the protein to peroxynitrite (Fig. 3 *A*). We observed significant changes in the ^1N-^{15}N HSQC spectrum upon exposure of the protein to peroxynitrite, in particular complete loss of some residues (notably Y16) and loss of intensity in others. Chemical-shift perturbation analysis showed large shifts for

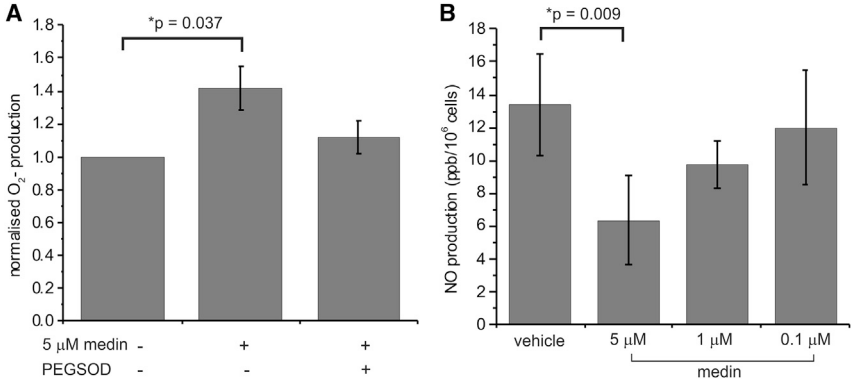

FIGURE 1 Effects of medin on NO and superoxide production from HUVECs. (*A*) Superoxide produced (hydroethidine fluorescence) after exposure to 5 μM medin (± PEGSOD) for 1 h relative to vehicle control; mean ± SEM is shown for $n = 5$. An increase in superoxide was observed upon addition of medin, attenuated by PEGSOD. (*B*) NO produced after exposure to medin (0.1–5 μM) for 20–24 h relative to vehicle control; mean ± SEM is shown for $n = 4$. A concentration-dependent decrease in NO was observed upon medin addition.

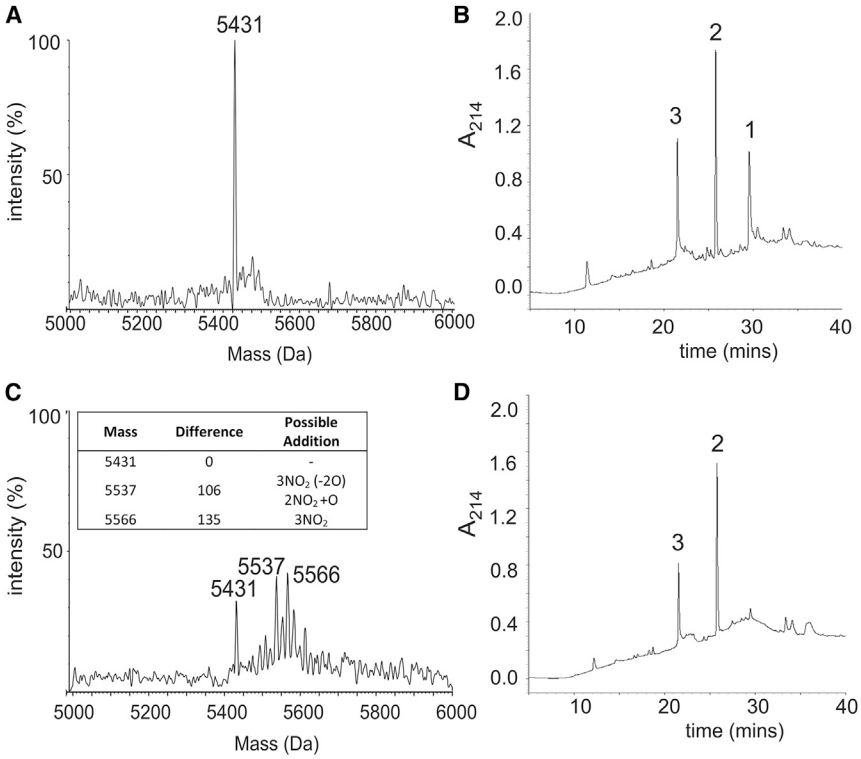

FIGURE 2 Confirmation of a change in mass after nitration. (*A*) The mass spectrum of control medin showed a single peak corresponding to the expected molecular weight of 5431. (*B*) RP-HPLC 5431 after trypsin digestion of control medin produced three peptides corresponding to residues 5–30, 31–41, and 42–50 (labeled 1, 2, and 3, respectively). (*C*) The mass spectrum of nitrated medin showed some nonmodified medin remaining, with additional peaks at 5537 and 5566 corresponding to the addition of NO_2 and O groups as suggested in the table inset. (*D*) RP-HPLC of trypsin-digested nitrated medin showed broadening of the peak corresponding to residues 5–30, peak 1. See Fig. S1 for confirmation of the presence of 3-nitrotyrosine.

residues surrounding Y16, in particular the neighboring residues S15 and G17 (Fig. 3 *B*, *dark box*). Notable changes (>1 SD away from the mean) were localized to a wider region surrounding Y16, spanning residues F8–V24 and incorporating the two tryptophan residues (Fig. 3 *B*, *lighter box*).

Corresponding ^{1}H-^{13}C aromatic CT-TROSY spectra mirrored the complete loss of Y16δ and ε peaks after exposure to peroxynitrite (Fig. 4 *A*), consistent with 3-nitrotyrosine formation (Fig. 4 *B*). Further changes were observed in peaks corresponding to tryptophan residues (11,21), including loss of intensity and minor shifts (Fig. 4 *A*). In contrast to tyrosine, tryptophan has several sites for possible modification (Fig. 4 *C*, *red*). Peaks corresponding to ζ_3 showed complete loss of intensity, suggesting that this site was modified (Fig. 4, *A* and *C*). However, peaks were not observed for ε_4 or ε_1, and shift changes were noted for ζ_2 and η; therefore, these cannot be ruled out as possible sites for NO_2 addition (Fig. 4 *C*). Additional signals exclusive to the aromatic spectrum for nitrated medin were consistent with predicted shifts for several nitrated species of tryptophan (Fig. 4 *A*, *red*). In contrast, phenylalanine peaks did not show a loss of intensity or shift (Fig. 4 *A*) indicative of a lack of modification of the bulk population.

To investigate whether nitration affected medin aggregation, we undertook an SRCD spectra analysis and investigated fibril morphology using AFM. After nitration, medin was buffer exchanged into aggregation buffer and incubated at 37°C for up to 48 h. ThT fluorescence presented an increase in lag time and reduced final fluorescence intensity for fibrillation of nitrated medin compared with control medin (Fig. 5 *A*). The SRCD spectra analysis showed that initially, medin and nitrated medin had similar secondary structure profiles (Fig. 5 *B*). However, upon aggregation, the spectra showed some differences, particularly at the lower wavelength, suggesting some change (albeit minor) in secondary structure (Fig. 5 *B*). AFM revealed that longer fibrils with a different morphology were formed after nitration (several micrometers in length) compared with control fibrils (up to 1 μm in length; Fig. 5 *C*). Control medin fibrils displayed height periodicity along the length of the fibrils (Fig. S2), whereas no periodicity was observed for nitrated samples, confirming a different morphology for fibrils formed from nitrated protein compared with control medin. Reduced final ThT fluorescence suggested fibrils with altered morphology in nitrated samples, consistent with the AFM analysis (Fig. 5, *A* and *C*). It is noted that the longer fibrils observed by AFM do not fit with the reduced β-sheet structure observed by SRCD; however, as SRCD only measures protein structure in solution, we speculate that the larger fibrils observed by AFM could be underrepresented in the SRCD analysis. Both freshly purified control and nitrated medin showed toxicity to human aortic smooth muscle cells, with ~80–85% cell viability (Fig. 5 *D*). After aggregation, control medin exhibited less toxicity to cells and ~90% cell viability was observed, consistent with previous findings (4,5). Aggregated nitrated medin showed enhanced cell toxicity compared with aggregated

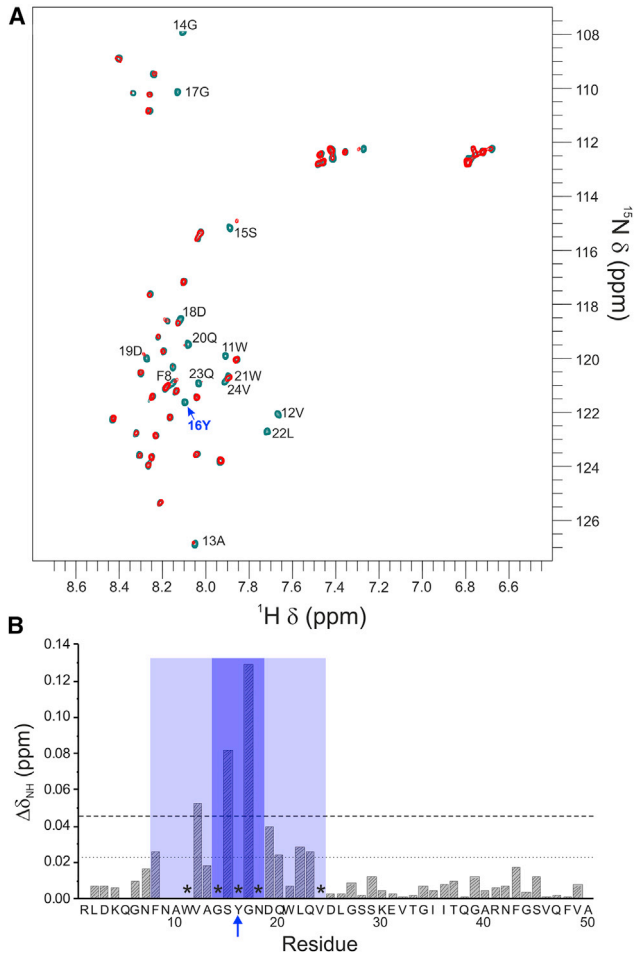

FIGURE 3 NMR spectra showed site-specific changes after nitration of medin. (*A*) Assigned ^{1}H-^{15}N HSQC spectra for control medin (*green*) and after exposure to peroxynitrite (*red*). Residues surrounding the site of nitration (Y16, *blue arrow*) are shown in bold. Spectra were collected in nitration buffer at pH 6.8 (100 mM potassium phosphate, 25 mM sodium bicarbonate, 0.1 mM diethylenetriaminepentaacetic acid). (*B*) Plot showing the chemical-shift (δ) differences between ^{1}H-^{15}N HSQC spectra for control and nitrated medin: 1 and 2 SDs from the mean are shown as dotted and dashed lines, respectively, and the asterisks indicate NH peaks that cannot be observed in the nitrated form. In the region immediately surrounding the site of nitration (G14-N18), all residues were >2 SDs or disappeared (*dark box*), and the region F8-V24 encompassing all shifts was >1 SD from the mean (*lighter box*).

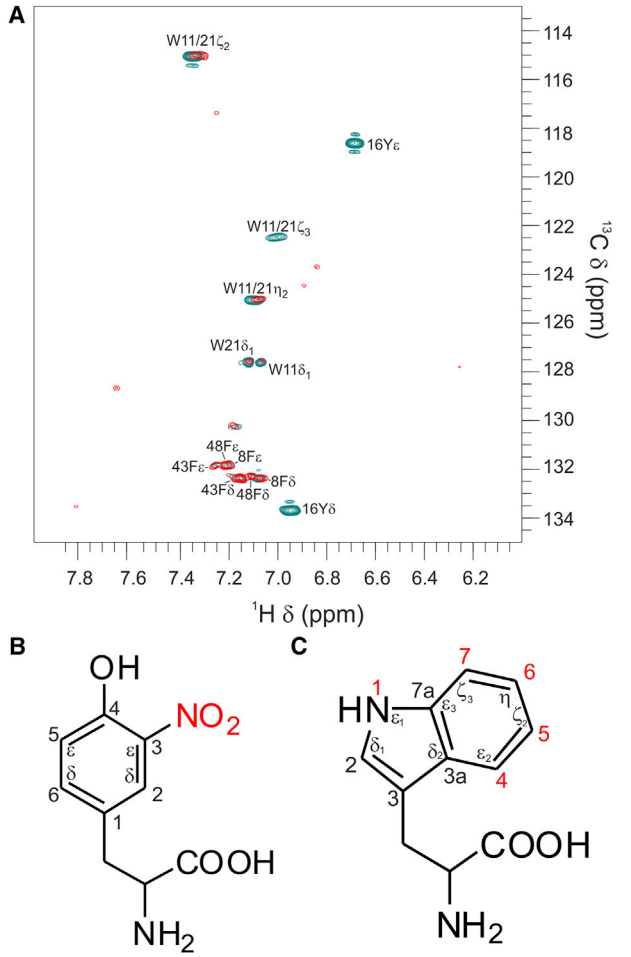

FIGURE 4 Site-specific changes of aromatic residues after nitration of medin. (*A*) ^{1}H-^{13}C aromatic CT-TROSY spectra for control medin (*green*) and after exposure to peroxynitrite (*red*). (*B*) Structure of 3-nitrotyrosine, with an additional NO_2 group shown in red. (*C*) Structure of tryptophan with possible sites for addition of NO_2 groups indicated by numbers in red.

control medin (Fig. 5 *D*). This difference was not significant; however, nitrated samples (freshly prepared and aggregated) showed increased variability in cell viability, leading to increased SEM values compared with control medin.

CONCLUSIONS

To investigate methods of manipulating the aggregation of medin and other amyloid proteins, it is essential to understand the residues that are involved in early interactions, since the aggregation intermediates of medin and other amyloid proteins are implicated in pathogenicity (5,38). Several approaches have been applied to probe soluble structures and the role of intermediate conformations for a range of amyloid proteins (39–43). However, a routine and robust method for obtaining site-specific structural information for soluble phases of amyloid-forming proteins is not readily available. Here, we used NMR to identify tyrosine and tryptophan side chains as the site of nitration of medin after exposure to peroxynitrite. Nitration hinders the rotation of the tyrosine ring, affecting its hydrogen-bonding ability and hydrophobicity. Tryptophan nitration is not as well documented as tyrosine nitration, possibly because tryptophan residues are more often found buried inside proteins (hydrophobicity index of 97 at pH 7), whereas tyrosine residues are more often surface exposed (hydrophobicity index of 63 at pH 7). This means that tyrosine residues are more readily available for nitration; however, surface-exposed tryptophan residues have been postulated to participate in the interaction of proteins with other molecules, suggesting that modification of tryptophan may modulate

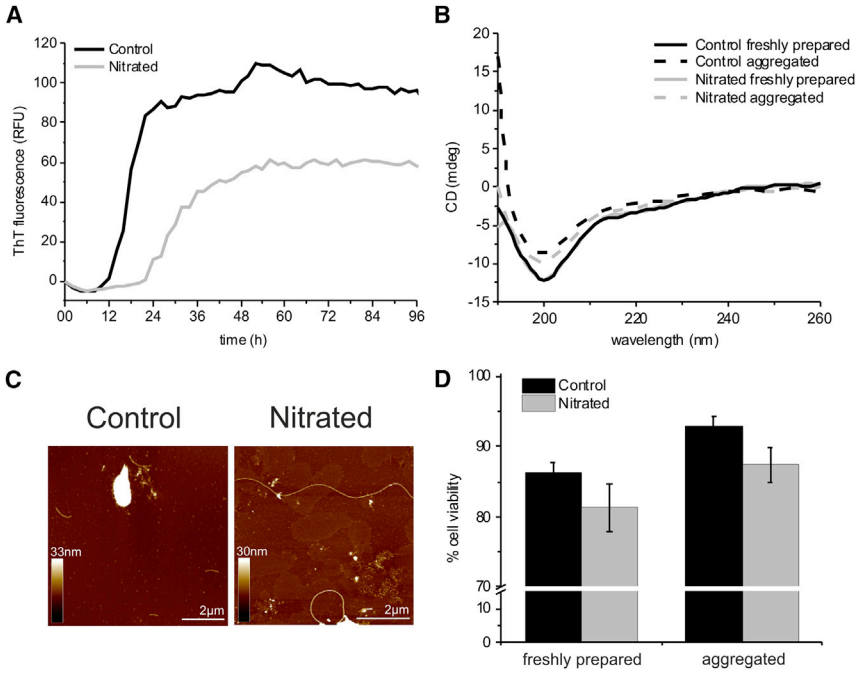

FIGURE 5 Aggregation of medin after exposure to peroxynitrite. (*A*) ThT fluorescence after aggregation of control (*black*) and nitrated (*gray*) medin over 48 h at 37°C, $n = 6$. (*B*) SRCD spectra for freshly prepared samples and after incubation for 48 h (aggregated). (*C*) AFM topographs for control and nitrated medin after incubation for 48 h at 37°C. See also Fig. S2 for periodicity measurements. (*D*) Cell viability of HAoSMC after exposure to freshly prepared and aggregated control and nitrated medin, as determined by CCK-8 assay; mean ± SEM is shown for $n = 5$. To see this figure in color, go online.

these interactions. The NMR data presented here suggest that medin is predominantly unfolded in its soluble form, and therefore all residues are likely to be accessible for nitration and oxidation.

The main aggregation-promoting region is thought to be the C-terminal 18–19 residues of medin (44). However, residues 9–14 and 20–23, which encompass most of the region shown here to have altered chemical shifts upon nitration (Fig. 3 *B*), have also been predicted to be aggregation-prone regions (45). Taken together, these observations suggest that interactions within this region may be the driving factor through which nitration alters the fibrillation kinetics and morphology of medin, and provide further avenues to investigate the aggregation mechanism of this protein.

Tyrosine nitration has been shown to lead to structural and functional changes in proteins, which can contribute to altered cell and tissue homeostasis (46). Previous experiments involving exposure of other amyloid-forming proteins (e.g., α-synuclein and tau) to nitrating agents in vitro showed altered aggregation pathways, with enhanced oligomerization (13,21) and reduced fibrillization (15,16). The data presented here are consistent with a similar mode of action of nitration on the aggregation of medin, with altered fibril morphology (ThT fluorescence and AFM) and enhanced toxicity to smooth muscle cells. Aneurysms often occur in the aorta because it gets too stiff and cannot cope with the stroke volume every time the heart pumps. We speculate that this enhanced toxicity may contribute to the pathology, with AMA in elastic lamina stiffening the artery, causing destruction of smooth muscle cells and thus leading to weakening of the vessel wall.

Various nitrated proteins have been identified in cardiovascular vessel walls, such as apolipoprotein B in aortic lesions (47). Here, we have shown that medin can induce oxidative stress conditions within HUVECs (Fig. 1), and that exposure to oxidative conditions alters the rate of medin aggregation in vitro and globally changes its structure and morphology, with alterations in toxicity. A similar induction of oxidative stress markers was previously observed and proposed as a pathogenic mechanism for amyloidogenic light-chain proteins (48). NMR is able to detect site-specific changes associated with posttranslational modifications (49–51). The NMR approaches described in this work elegantly demonstrate how this technique can detect sites of chemical modification and identify which regions of the protein are responsible for causing protein aggregation, and hence provide, to our knowledge, a new avenue for exploring the involvement of ROS and RNS in AMA deposition.

SUPPORTING MATERIAL

Supporting Materials and Methods and two figures are available at http://www.biophysj.org/biophysj/supplemental/S0006-3495(15)01110-8.

AUTHOR CONTRIBUTIONS

H.A.D. produced the protein and carried out the majority of the experimental work. M.M.P. advised and assisted with the NMR experiments. M.C.W. carried out the mass spectrometry and HPLC analysis. R.Q.M., S.T., and D.A.F. collected the superoxide and NO data. L.-N.L. performed the AFM. C.J.L. was an MBiolSci student who carried out a preliminary nitration analysis. J.M. instigated all of the work, collated data, and wrote the manuscript.

ACKNOWLEDGMENTS

We acknowledge the Diamond Light Source (Oxford, UK) for providing access to beamline B23 (SM8979), which contributed to the results presented here, and the Oxford Protein Production Facility (UK) for assistance with protein expression optimization.

Financial support for this work was provided by the British Heart Foundation (FS/12/61/29877 to J.M. and H.A.D.), a VA Merit award (I01BX007080), the National Institute on Aging (1R21AG044723), the Amyloidosis Foundation (R.Q.M., S.T., and D.A.F.), a Royal Society University Research Fellowship (UF120411 to L.-N.L.), a research grant for the University Research Fellowship (RG130442 to L.-N.L.), and a Biotechnology and Biological Sciences Research Council grant (BB/M024202/1 to L.-N.L.). This work was also supported by an award from the University of Liverpool Technology Directorate Voucher Scheme and the NMR Centre for Structural Biology.

REFERENCES

1. Peng, S. W., G. T. Westermark, …, P. Westermark. 2001. Distribution of medin-amyloid in aging and in association with arterial diseases. *Amyloid.* 8:122–123.
2. Mucchiano, G., G. G. I. Cornwell, 3rd, and P. Westermark. 1992. Senile aortic amyloid. Evidence for two distinct forms of localized deposits. *Am. J. Pathol.* 140:871–877.
3. Häggqvist, B., J. Näslund, …, P. Westermark. 1999. Medin: an integral fragment of aortic smooth muscle cell-produced lactadherin forms the most common human amyloid. *Proc. Natl. Acad. Sci. USA.* 96:8669–8674.
4. Madine, J., and D. A. Middleton. 2010. Comparison of aggregation enhancement and inhibition as strategies for reducing the cytotoxicity of the aortic amyloid polypeptide medin. *Eur. Biophys. J.* 39:1281–1288.
5. Peng, S., A. Larsson, …, P. Westermark. 2007. Role of aggregated medin in the pathogenesis of thoracic aortic aneurysm and dissection. *Lab. Invest.* 87:1195–1205.
6. Sies, H. 1991. Oxidative stress: from basic research to clinical application. *Am. J. Med.* 91 (3C):31S–38S.
7. Peluffo, G., and R. Radi. 2007. Biochemistry of protein tyrosine nitration in cardiovascular pathology. *Cardiovasc. Res.* 75:291–302.
8. Zhang, M., and A. M. Shah. 2014. ROS signalling between endothelial cells and cardiac cells. *Cardiovasc. Res.* 102:249–257.
9. Dröge, W. 2002. Free radicals in the physiological control of cell function. *Physiol. Rev.* 82:47–95.
10. Beckmann, J. S., Y. Z. Ye, …, C. R. White. 1994. Extensive nitration of protein tyrosines in human atherosclerosis detected by immunohistochemistry. *Biol. Chem. Hoppe Seyler.* 375:81–88.
11. Chen, C. L., J. Chen, …, Y. R. Chen. 2008. Protein tyrosine nitration of the flavin subunit is associated with oxidative modification of mitochondrial complex II in the post-ischemic myocardium. *J. Biol. Chem.* 283:27991–28003.
12. Xu, S., J. Ying, …, R. A. Cohen. 2006. Detection of sequence-specific tyrosine nitration of manganese SOD and SERCA in cardiovascular disease and aging. *Am. J. Physiol. Heart Circ. Physiol.* 290:H2220–H2227.
13. Reynolds, M. R., R. W. Berry, and L. I. Binder. 2005. Site-specific nitration and oxidative dityrosine bridging of the tau protein by peroxynitrite: implications for Alzheimer's disease. *Biochemistry.* 44:1690–1700.
14. Kummer, M. P., M. Hermes, …, M. T. Heneka. 2011. Nitration of tyrosine 10 critically enhances amyloid β aggregation and plaque formation. *Neuron.* 71:833–844.
15. Yamin, G., V. N. Uversky, and A. L. Fink. 2003. Nitration inhibits fibrillation of human alpha-synuclein in vitro by formation of soluble oligomers. *FEBS Lett.* 542:147–152.
16. Uversky, V. N., G. Yamin, …, A. L. Fink. 2005. Effects of nitration on the structure and aggregation of alpha-synuclein. *Brain Res. Mol. Brain Res.* 134:84–102.
17. Duda, J. E., B. I. Giasson, …, J. Q. Trojanowski. 2000. Widespread nitration of pathological inclusions in neurodegenerative synucleinopathies. *Am. J. Pathol.* 157:1439–1445.
18. Reynolds, M. R., J. F. Reyes, …, L. I. Binder. 2006. Tau nitration occurs at tyrosine 29 in the fibrillar lesions of Alzheimer's disease and other tauopathies. *J. Neurosci.* 26:10636–10645.
19. Shishehbor, M. H., R. J. Aviles, …, S. L. Hazen. 2003. Association of nitrotyrosine levels with cardiovascular disease and modulation by statin therapy. *JAMA.* 289:1675–1680.
20. Davies, H. A., M. C. Wilkinson, …, D. A. Middleton. 2014. Expression and purification of the aortic amyloid polypeptide medin. *Protein Expr. Purif.* 98:32–37.
21. Souza, J. M., B. I. Giasson, …, H. Ischiropoulos. 2000. Dityrosine cross-linking promotes formation of stable α-synuclein polymers. Implication of nitrative and oxidative stress in the pathogenesis of neurodegenerative synucleinopathies. *J. Biol. Chem.* 275:18344–18349.
22. Ischiropoulos, H., and A. B. al-Mehdi. 1995. Peroxynitrite-mediated oxidative protein modifications. *FEBS Lett.* 364:279–282.
23. Vranken, W. F., W. Boucher, …, E. D. Laue. 2005. The CCPN data model for NMR spectroscopy: development of a software pipeline. *Proteins.* 59:687–696.
24. Davies, H. A., M. M. Phelan, and J. Madine. 2015. ^{1}H, ^{15}N and ^{13}C assignment of the amyloidogenic protein medin using fast-pulsing NMR techniques. *Biomol. NMR Assign.* Published online September 16, 2015. http://dx.doi.org/10.1007/s12104–015–9641-z.
25. Hussain, R., T. Jávorfi, and G. Siligardi. 2012. Circular dichroism beamline B23 at the Diamond Light Source. *J. Synchrotron Radiat.* 19:132–135.
26. Liu, L.-N., K. Duquesne, …, S. Scheuring. 2011. Forces guiding assembly of light-harvesting complex 2 in native membranes. *Proc. Natl. Acad. Sci. USA.* 108:9455–9459.
27. Beckman, J. S., J. Chen, …, J. P. Crow. 1994. Oxidative chemistry of peroxynitrite. *Methods Enzymol.* 233:229–240.
28. Dikalov, S., K. K. Griendling, and D. G. Harrison. 2007. Measurement of reactive oxygen species in cardiovascular studies. *Hypertension.* 49:717–727.
29. Zhao, H., J. Joseph, …, B. Kalyanaraman. 2005. Detection and characterization of the product of hydroethidine and intracellular superoxide by HPLC and limitations of fluorescence. *Proc. Natl. Acad. Sci. USA.* 102:5727–5732.
30. Didion, S. P., and F. M. Faraci. 2005. Ceramide-induced impairment of endothelial function is prevented by CuZn superoxide dismutase overexpression. *Arterioscler. Thromb. Vasc. Biol.* 25:90–95.
31. Kanamori, A., M. M. Catrinescu, …, L. A. Levin. 2010. Superoxide is an associated signal for apoptosis in axonal injury. *Brain.* 133:2612–2625.
32. Liu, Z., J. Cao, …, Y. Xue. 2011. GPS-YNO2: computational prediction of tyrosine nitration sites in proteins. *Mol. Biosyst.* 7:1197–1204.
33. Gow, A., D. Duran, …, H. Ischiropoulos. 1996. Carbon dioxide enhancement of peroxynitrite-mediated protein tyrosine nitration. *Arch. Biochem. Biophys.* 333:42–48.
34. Alvarez, B., H. Rubbo, …, R. Radi. 1996. Peroxynitrite-dependent tryptophan nitration. *Chem. Res. Toxicol.* 9:390–396.
35. Yamakura, F., and K. Ikeda. 2006. Modification of tryptophan and tryptophan residues in proteins by reactive nitrogen species. *Nitric Oxide.* 14:152–161.
36. Sarver, A., N. K. Scheffler, …, B. W. Gibson. 2001. Analysis of peptides and proteins containing nitrotyrosine by matrix-assisted laser desorption/ionization mass spectrometry. *J. Am. Soc. Mass Spectrom.* 12:439–448.
37. Yamakura, F., T. Matsumoto, …, K. Takamori. 2005. Nitrated and oxidized products of a single tryptophan residue in human

Cu,Zn-superoxide dismutase treated with either peroxynitrite-carbon dioxide or myeloperoxidase-hydrogen peroxide-nitrite. *J. Biochem.* 138:57–69.

38. Fändrich, M. 2012. Oligomeric intermediates in amyloid formation: structure determination and mechanisms of toxicity. *J. Mol. Biol.* 421:427–440.
39. Eichner, T., A. P. Kalverda, …, S. E. Radford. 2011. Conformational conversion during amyloid formation at atomic resolution. *Mol. Cell.* 41:161–172.
40. Mishra, R., M. Geyer, and R. Winter. 2009. NMR spectroscopic investigation of early events in IAPP amyloid fibril formation. *ChemBioChem.* 10:1769–1772.
41. Vivekanandan, S., J. R. Brender, …, A. Ramamoorthy. 2011. A partially folded structure of amyloid-beta(1-40) in an aqueous environment. *Biochem. Biophys. Res. Commun.* 411:312–316.
42. Svane, A. S. P., K. Jahn, …, N. C. Nielsen. 2008. Early stages of amyloid fibril formation studied by liquid-state NMR: the peptide hormone glucagon. *Biophys. J.* 95:366–377.
43. Hou, L., H. Shao, …, M. G. Zagorski. 2004. Solution NMR studies of the A beta(1-40) and A beta(1-42) peptides establish that the Met35 oxidation state affects the mechanism of amyloid formation. *J. Am. Chem. Soc.* 126:1992–2005.
44. Larsson, A., L. Söderberg, …, P. Westermark. 2007. Unwinding fibril formation of medin, the peptide of the most common form of human amyloid. *Biochem. Biophys. Res. Commun.* 361:822–828.
45. Davies, H. A., J. Madine, and D. A. Middleton. 2012. Solid-state NMR reveals differences in the packing arrangements of peptide aggregates derived from the aortic amyloid polypeptide medin. *J. Pept. Sci.* 18:65–72.
46. Radi, R. 2013. Protein tyrosine nitration: biochemical mechanisms and structural basis of functional effects. *Acc. Chem. Res.* 46:550–559.
47. Leeuwenburgh, C., M. M. Hardy, …, J. W. Heinecke. 1997. Reactive nitrogen intermediates promote low density lipoprotein oxidation in human atherosclerotic intima. *J. Biol. Chem.* 272:1433–1436.
48. Migrino, R. Q., S. Truran, …, P. Hari. 2011. Human microvascular dysfunction and apoptotic injury induced by AL amyloidosis light chain proteins. *Am. J. Physiol. Heart Circ. Physiol.* 301:H2305–H2312.
49. Díaz-Moreno, I., J. M. García-Heredia, …, M. A. De la Rosa. 2013. Recent methodological advances in the analysis of protein tyrosine nitration. *ChemPhysChem.* 14:3095–3102.
50. Liokatis, S., A. Dose, …, P. Selenko. 2010. Simultaneous detection of protein phosphorylation and acetylation by high-resolution NMR spectroscopy. *J. Am. Chem. Soc.* 132:14704–14705.
51. Kosten, J., A. Binolfi, …, P. Selenko. 2014. Efficient modification of alpha-synuclein serine 129 by protein kinase CK1 requires phosphorylation of tyrosine 125 as a priming event. *ACS Chem. Neurosci.* 5:1203–1208.